Structure of the Integrin β3 Transmembrane Segment in Phospholipid Bicelles and Detergent Micelles[†]

Tong-Lay Lau,[‡] Anthony W. Partridge,[§] Mark H. Ginsberg,[§] and Tobias S. Ulmer*[,‡]

Department of Biochemistry and Molecular Biology and Zilkha Neurogenetic Institute, Keck School of Medicine, University of Southern California, 1501 San Pablo Street, Los Angeles, California 90033, and Department of Medicine, University of California, San Diego, 9500 Gilman Drive, La Jolla, California 92093

Received January 19, 2008; Revised Manuscript Received February 12, 2008

ABSTRACT: Integrin adhesion receptors transduce bidirectional signals across the plasma membrane, with the integrin transmembrane domains acting as conduits in this process. Here, we report the first high-resolution structure of an integrin transmembrane domain. To assess the influence of the membrane model system, structure determinations of the β3 integrin transmembrane segment and flanking sequences were carried out in both phospholipid bicelles and detergent micelles. In bicelles, a 30-residue linear α-helix, encompassing residues I693−H772, is adopted, of which I693-I721 appear embedded in the hydrophobic bicelle core. This relatively long transmembrane helix implies a pronounced helix tilt within a typical lipid bilayer, which facilitates the snorkeling of K716's charged side chain out of the lipid core while simultaneously immersing hydrophobic L717−I721 in the membrane. A shortening of bicelle lipid hydrocarbon tails does not lead to the transfer of L717−I721 into the aqueous phase, suggesting that the reported embedding represents the preferred β3 state. The nature of the lipid headgroup affected only the intracellular part of the transmembrane helix, indicating that an asymmetric lipid distribution is not required for studying the β3 transmembrane segment. In the micelle, residues L717−I721 are also embedded but deviate from linear α-helical conformation in contrast to I693−K716, which closely resemble the bicelle structure.

Integrins are a large family of heterodimeric adhesion receptors that bind to extracellular matrix proteins, serum proteins, and coreceptors expressed on the cell surface (*1*). Many integrins exist in a default low affinity state, and their conversion to the activated form, following the transmission of an activating signal from the cytoplasmic to extracellular domains (inside-out signaling), is vital to an array of physiological processes such as cell migration, extracellular matrix assembly and pathological processes such as inflammation, thrombosis, and tumor metastasis (*1*). Mutational studies of integrin αIIb-β3 suggested that sequence-specific hydrophobic packing of the transmembrane (TM[1]) helices and adjacent electrostatic αIIb-β3 interactions on the cytosolic side stabilize the inactive state (*2*–*6*). Integrin occupancy by extracellular ligands can also lead to biochemical signaling events and the interaction of integrins with the actin cytoskeleton (outside-in signaling), processes essential to cell adhesion, migration, and anchorage dependent cell growth and survival (*1*). Mutational and pharmacological studies have suggested that the disruption of the intersubunit association is also important in this form of signaling (*7, 8*). Thus, a large body of indirect evidence supports the hypothesis that the integrin transmembrane domains play a direct role in bidirectional integrin signaling.

Each α and β integrin subunit consists of a large extracellular domain, a single pass transmembrane helix, and a short, C-terminal cytoplasmic tail (*1*). Across family members and species, the transmembrane helices have a conserved but unusual pattern of hydrophobicity. Each helix contains a stretch of 23 mostly hydrophobic residues that terminates on the intracellular side with a Trp-Lys pair, or similar residue combination. These two residues are followed by a second stretch of several mostly apolar residues (*9*). While the first segment alone represents an efficient stop−transfer sequence, the snorkeling capability of the long lysine side chain in combination with an unknown membrane-crossing angle make the topology of the second segment controversial. Predictive methods suggest it to be cytoplasmic; however, glycosylation mapping studies in microsomal membranes indicate that it may be membrane-embedded (*10*). These indirect methods have been complemented by the secondary structure characterization of the integrin β3 TM helix in micelles (*11*). However, the lack of direct structural and topological information concerning the TM helices has so far impeded an in-depth understanding of the signaling events within the membrane. As a starting step, the topology and atomic resolution structure of a peptide corresponding

[†] This work was supported by an award from the American Heart Association to T.S.U. and by Grants from the National Institutes of Health to M.H.G. T.L.L. is a recipient of a postdoctoral fellowship from the American Heart Association. A.P. was a postdoctoral fellow of the Tobacco Diseases Related Program of California.

* Corresponding author. Tel: 323-442-4326. Fax: 323-442-4404. E-mail: tulmer@usc.edu.

[‡] University of Southern California.

[§] University of California, San Diego.

[1] Abbreviations: DHPC, 1,2-dihexanoyl-*sn*-glycero-3-phosphocholine; DPC, dodecylphosphocholine; POPC, 1-palmitoyl-2-oleoyl-*sn*-glycero-3-phosphocholine; TM, transmembrane.

10.1021/bi800107a CCC: $40.75
Published on Web 03/06/2008

to the β3 transmembrane segment and flanking sequences are reported here.

Structural studies of integral membrane proteins are complicated by the appropriate selection of a membrane model system. This seems particularly relevant for single TM helices since all side chains are exposed to the membrane environment in contrast to proteins composed of multiple TM helices. To assess the implication of the membrane model system, the β3 TM structure and topology have been determined in two media, detergent micelles and phospholipid bicelles. Micelles are composed of detergent-like molecules and generally form approximately spherical particles with a relatively invariant number of detergent molecules (aggregation number) and, hence, size. Following the previous integrin β3 TM study (*11*), dodecylphosphocholine (DPC) micelles are used and are referred to simply as micelles. Bicelles comprise a small, symmetric lipid bilayer whose rim is stabilized by short-chain lipids (*12, 13*). The molar ratio of long-chain to short-chain lipids, the q-factor, determines the size of the bicelle bilayer and, hence, the overall size of the bicelle. In the following, the term bicelle is simply used for a $q = 0.3$ bicelle composed of glycerophosphatitylcholine-based lipids of 16/18 carbon atom tails (1-palmitoyl-2-oleoyl-*sn*-glycero-3-phosphocholine, POPC) and 6/6 tails (1,2-dihexanoyl-*sn*-glycero-3-phosphocholine, DHPC). It is well documented that bicelles of this q-factor form magnetically isotropic particles that exhibit planar geometry (*14, 15*) characteristic of a small, central long-chain lipid bilayer surrounded by short-chain lipids. Using the bicelle system, we also investigated the effect of the lipid headgroup type on the β3 TM structure and evaluated the appropriateness of an only symmetric lipid distribution. Thus, a detailed analysis of the impact of membrane model systems on helical TM structure is presented, which provides general insight into lipid–protein interactions.

Overall, the analysis revealed a strong preference of β3 residues I693-I721 to immerse into the hydrophobic bicelle core, implying a pronounced helix tilt relative to a typical membrane for this 29-residue segment exhibiting linear α-helical structure. The bicelle- and micelle-embedded β3 structures differ significantly because of perceived shortcomings of the micelle environment. The impact of lipid type headgroup and lipid symmetry strongly imply that the reported bicelle-embedded β3 structure corresponds to the native, monomeric β3 TM segment and, therefore, forms the basis for understanding its association with the αIIb TM segment and conformational changes that occur during integrin activation. Moreover, the definition of the β3 structure at the membrane−water interface is crucial for understanding β3 membrane-proximal interactions with cytosolic proteins, such as talin, that effect integrin αIIb-β3 activation (*16, 17*).

EXPERIMENTAL PROCEDURES

Integrin β3 Expression and Purification. Synthetic oligonucleotides coding for human integrin β3 residues P685-F727 were assembled by PCR and subcloned into the pET-31 expression vector (Novagen, Inc.) with ketosteroid isomerase (KSI) as N-terminal fusion protein. To avoid peptide aggregation, a C687S substitution was incorporated. Expression was induced in *E. coli* BL21(DE3)pLysS,T1^R cells (Sigma-Aldrich, Inc.) growing in M9 minimal medium at 37 °C at an OD_{600} of 1.0 by adding IPTG to 1.0 mM. $^2H/^{13}C/^{15}N$ isotope labeling was achieved by employing 99% ^{13}C-D glucose and 99% $^{15}NH_4Cl$ in 99% D_2O cultures. Cells were harvested by centrifugation 5 h after induction and lysed by sonication in 50 mM Tris·HCl, pH 8.0, 300 mM NaCl, 100 mM SDS, 20 mM imidazole, and 2 mM β-mercaptoethanol. The clarified lysate was applied on a HiTrap Chelating HP column (GE Amersham, Inc.) charged with Ni^{2+} for immobilized metal affinity chromatography (IMAC). The column was washed with 50 mM Tris·HCl, pH 8.0, 300 mM NaCl, and 25 mM SDS, followed by buffer exchange into 50 mM Tris·HCl, pH 8.0, 300 mM NaCl, 8 M urea, and 20 mM imidazole and additional washing with an elevated imidazole concentration of 50 mM. After another buffer exchange into 50 mM Tris·HCl, pH 8.0, 300 mM NaCl, 6 M guanidine·HCl, and 20 mM imidazole, bound protein was eluted by raising the imidazole concentration to 300 mM. Following ref *18*, the β3 peptide was subsequently cleaved from the fusion protein using the intervening acid-labile Asp-Pro peptide bond in 10% formic acid for 120 min at 80 °C, leaving P685 as the N-terminal β3 residue. The β3 peptide was purified by reversed-phase HPLC on a Hamilton PRP-3 column at 60 °C using a linear gradient from 35%/65% buffer A (H_2O, 0.1% TFA)/buffer B (80% Acetonitrile, 20% 1-propanol 0.1% TFA) to 80%/20% in 45 min. Peptide purity and mass were verified by SDS−PAGE and electrospray mass spectrometry.

NMR Sample Preparation. Freeze-dried peptide was taken up in 320 μL bicelle or micelle solution to give a β3 peptide concentration of ~0.6 mM. Unless otherwise stated, bicelles comprised 350 mM DHPC and 105 mM POPC, which resulted in a q-factor of 0.3. Micelles were made up of 450 mM DPC. The solutions were buffered by 25 mM NaH_2PO_4/Na_2HPO_4, pH 6.5, in the presence of 6% D_2O and 0.02% w/v NaN_3, unless otherwise stated. To illustrate the spectral quality obtained, H-N TROSY spectra of bicelle- and micelle-embedded β3 are shown in Supporting Information, Figure 1.

To align the β3-bicelle/micelle complexes relative to the magnetic field stretched, negatively charged polyacrylamide gels were used (*19, 20*). For the β3-micelle complex, a 320 μL gel was polymerized in 150 mM Tris·HCl, pH 8.0, from a 5.6% w/v solution of acrylamide (AA), 2-acrylamido-2-methyl-1-propanesulfonate (AMPS) and bisacrylamide (BIS) with a monomer-to-cross-linker ratio of 49:1 (w/w) and a molar ratio of 96:4 of AA to AMPS. For easier comparisons between gels, AMPS is counted as AA in the stated weight ratios (*21*). For the β3-bicelle complex, two gels of 320 μL volume were prepared using a monomer-to-cross-linker ratio of 49:1 (w/w) and a molar ratio of 94:6 of AA to AMPS. The first gel was polymerized from a 4.6% w/v solution of AA, AMPS, and BIS, whereas a 4.2% solution was used for the second gel. All gels were dialyzed overnight in 50 mL of 100 mM NaH_2PO_4/Na_2HPO_4, pH 6.8, followed by H_2O for 10 h and another H_2O dialysis overnight. Following the complete drying of the gels, they were soaked in 320 μL of β3-bicelle/micelle solution for 24 h and transferred into open-ended NMR tubes as described (*22*). For the 4.2% bicelle gel, the β3 buffer was varied to 25 mM NaH_2PO_4/Na_2HPO_4, pH 7.4, and 0.02% w/v NaN_3. The following ^2H splittings were observed: 3.2 Hz (β3-micelle gel at 25 °C), 2.1 Hz

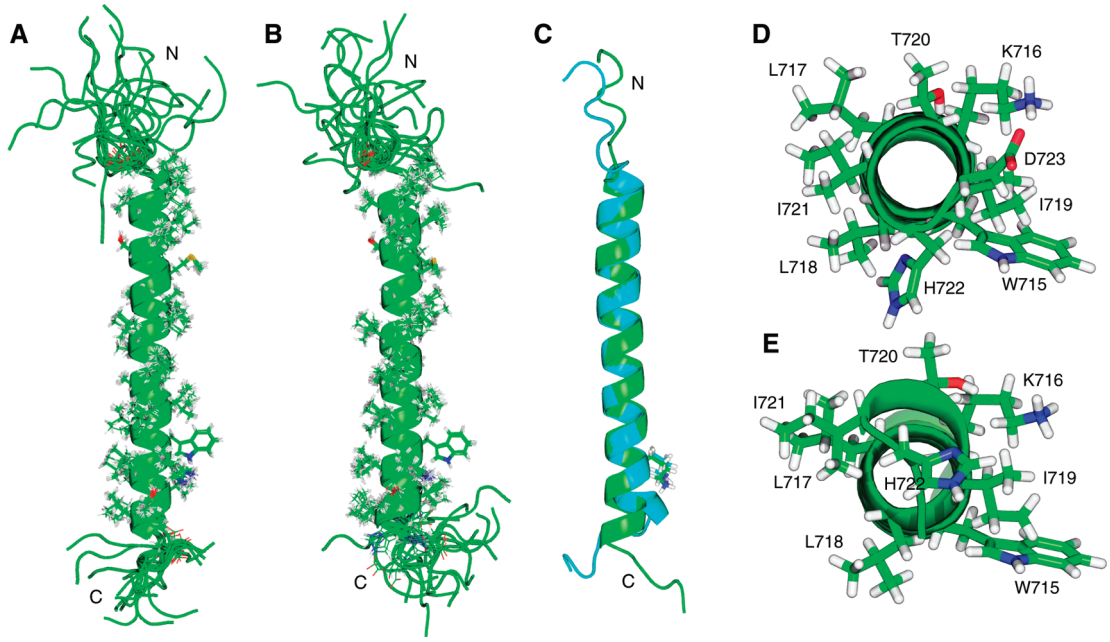

FIGURE 1: Structure of the integrin β3 transmembrane segment in bicelles and micelles. (A and B) Superposition of the ensemble of all 20 calculated simulated annealing structures of (A) bicelle- and (B) micelle-embedded β3. (C) Overlay of the energy-minimized, average structures of bicelle- and micelle-embedded β3 shown in *green* and *cyan*, respectively. The C^{α}, C′, and N backbone coordinates of I693-K716 were minimized between the two structures (rmsd 0.33 Å). The side chain of K716 is shown in ball-and-stick representation. The helix of bicelle-embedded β3 is one residue longer than its micellar counterpart. (D and E) View along the helix axis from the C-terminal side. The side chains of W715-D723 are shown in ball-and-stick representation. In contrast to bicelle-embedded β3, shown in (D), no well-defined conformation was obtained for D723 within the micelle environment, shown in (E), and D723 is therefore omitted.

(4.6% β3-bicelle gel at 40 °C), and 1.6 Hz (4.2% β3-bicelle gel at 40 °C).

Preparation of Mn^{2+}EDDA. To use paramagnetic Mn^{2+} without a partitioning bias near polar protein and lipid/detergent functional groups, it was used in complex with the chelating agent $EDDA^{2-}$ (ethylenediamine-*N*,*N*′-diacetate). A 0.5 M Na_2EDDA solution was combined with a predefined amount of $MnCl_2$ for a final $Mn^{2+}EDDA^{2-}$ concentration of 0.5 M and vortexed immediately until a clear solution was obtained. White $Mn^{2+}EDDA^{2-}$ began to precipitate from the solution within a minute. The pelleted complex was washed twice with methanol, followed by ethanol and air-dried. Twenty-five millimolar $Mn^{2+}EDDA^{2-}$ stock solutions were prepared freshly in 25 mM HEPES·NaOH, pH 7.0, and 0.02% NaN_3 buffer.

NMR Spectroscopy. NMR experiments were carried out on a cryoprobe-equipped Bruker Avance 700 spectrometer at 25 °C, except for the gel-aligned bicelle samples, which were measured at 40 °C. Data were processed and analyzed with the nmrPipe package (*23*) and CARA. Throughout all experiments, the solvent was kept at $+I_z$ whenever possible and TROSY-type H-N detection was used (*24*). H^N, N, C^{α}, C^{β}, and C′ assignments were made from HNCA, HNCACB, HNCO, and HN(CA)CO experiments. H^N-H^N NOEs were measured using HSQC-NOESY-TROSY experiments with a mixing time of 150 ms. $^3J_{C'C\gamma}$ and $^3J_{NC\gamma}$ couplings for aromatic and aliphatic residues were obtained from quantitative *J* -correlation spectroscopy (*25*) with dephasing times of 50 and 100 ms, respectively. $^1J_{NH}$, $^1J_{C\alpha C'}$, $^1J_{C'N}$, and $^1J_{NH}+^1D_{NH}$, $^1J_{C\alpha C'}+^1D_{C\alpha C'}$, $^1J_{C'N}+^1D_{C'N}$ couplings were determined from $^1J_{NH}$-scaled HNCO experiments (*26*) and from quantitative *J*-correlation HNCO experiments (*27, 28*) on isotropic and aligned samples, respectively. $\{^1H\}$-^{15}N NOE measurements were carried out using 5 s of presaturation preceded by a recycling delay of 4 s for the NOE experiment and a 9 s recycle delay for the reference experiment.

Structure Calculations. Structures of the folded regions of the β3 peptide (residues D692-D723 for bicelle- and D692-H722 for micelle-embedded β3, respectively, c.f. Figure 2B) were calculated by simulated annealing starting at 3000 K using the program XPLOR-NIH (*29*). The peptide termini were represented by random-coil conformations. The difference between predicted and experimental residual dipolar couplings was described by a quadratic harmonic potential. Dihedral angle restraints were implemented using a quadratic square-well potential and were merely aiding in the convergence of the residual dipolar coupling restraints (RDCs). φ, θ backbone dihedral angle constraints were extracted from N, C^{α}, C^{β} and C′ chemical shifts using the program TALOS (*30*). χ_1 side-chain angle restraints were derived from the $^3J_{C'C\gamma}$ and $^3J_{NC\gamma}$ coupling constants (Supporting Information, Table 2). Backbone−backbone H^N-H^N NOE distance restraints did not restrict β3 conformations beyond general helical conformational space. A backbone−backbone hydrogen-bonding potential was used (*31*). A torsion angle potential of mean force (*32*), which was modified to implement the preferred rotamers in transmembrane helices (*33, 34*), was employed. Moreover, the higher side chain rotamers (χ_2-χ_4) of K716 were selected to extend toward the C-terminus, i.e., to snorkel. An ensemble of a total of 20 structures was calculated (Supporting Information, Table 1). The structures have been deposited in the Protein Data Bank (accession numbers 2rmz and 2rn0 for bicelle- and micelle-embedded β3, respectively) along with their energy-minimized average structures.

RESULTS AND DISCUSSION

Structure of Bicelle- and Micelle-Embedded β3. The structure of the β3 transmembrane segment embedded in bicelles and micelles, respectively, was determined by multidimensional heteronuclear NMR spectroscopy, making use of a $^{2}H/^{13}C/^{15}N$ labeled peptide encompassing residues P685-F727. At the employed peptide-to-detergent ratio, the β3 peptide is monomeric (*35*). Likewise, as judged from examining spectral properties such as peak position, line width, and number of peaks as a function of peptide-to-bicelle ratio (data not shown), monomeric peptide was obtained within the employed bicelle environment. This is in good agreement with the very weak β3 homo-oligomerization tendency in *E. coli* cell membranes (*36*). Moreover, no discernible differences in H-N chemical shifts were detected between bicelle q-factors of 0.2 to 0.3 (data not shown), suggesting that the peptide interacts exclusively with the long-chain lipids of the bicelle. Structure calculations relied on relating backbone internuclear bond vector orientations relative to a common molecular alignment frame (*37*), with the β3 chemical shift patterns providing additional backbone dihedral angle restraints (*30*). For the ensemble of 20 calculated simulated annealing structures, coordinate precisions of 0.18 and 0.21 Å were obtained for the backbone-heavy atoms of the structured regions of the bicelle- and micelle-embedded β3 peptide, respectively. The structural statistics are summarized in Supporting Information, Table 1.

The structure of bicelle-embedded β3 consists of a linear α-helix extending from I693 to H722 (Figure 1A). N-terminal to D692 on the extracellular side and C-terminal to D723 on the intracellular side, the peptide becomes dynamically unstructured. The inclusion of the entire intracellular tail, terminating at T762, does not affect the transmembrane structure, as judged from the small D692-D723 chemical shift changes encountered when extending the β3 peptide (Supporting Information, Figure 2). For micelle-embedded β3, a highly similar structure was obtained for I693-K716 (Figure 1B and C). Relative to the bicelle-embedded structure, this region exhibits a backbone rmsd of 0.33 Å. However, C-terminal to K716, the first charged residues on the intracellular side, the structures differ markedly. The linear α-helical conformation of the mostly hydrophobic L717-I721 residues found in bicelle-embedded β3 is distorted in the micelle environment, and the helix terminates at I721 instead of H722 (Figure 1C−E). Nevertheless, L717-I721 backbone torsion angles are still within the most favorable region of the Ramachandran plot (Supporting Information, Table 1). The distortion results in the bending of the last helix turns away from the helix axis and in a slightly reduced helical rise per residue for L717-I721. An overall shortening of the micelle- compared to the bicelle-embedded TM helix by approximately 0.5 Å along the helix axis results. As a further consequence, the β3 side-chain orientations differ significantly between the two media for residues following K716 (Figure 1D and E). For both bicelle- and micelle-embedded β3, the averaging of side chain χ_1 rotameric states is common (Supporting Information, Table 2). One interesting difference between the χ_1 distributions between the two media is found for W715. Its rotameric state is well defined within the bicelle, but not the micelle.

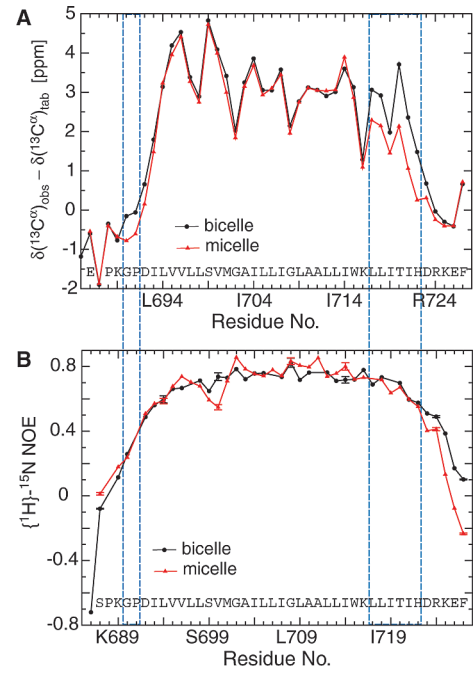

FIGURE 2: Comparison of backbone structural and dynamic parameters for the β3 transmembrane segment in bicelles and micelles. (A) The β3 sary $^{13}C^{\alpha}$ chemical shifts obtained in the two media are compared. Besides their congruence for I693-K716 and divergence for L717-H722, a small shift difference of ~0.5 ppm was observed for residues G690-P691. Although the G690-P691 sary $^{13}C^{\alpha}$ chemical shifts are already close to random-coil values, i.e., zero, the difference between bicelle- and micelle-embedded β3 suggests that slightly different ensembles of G690-P691 conformers were obtained at the bicelle− and micelle−water interface, respectively. The glycine−proline combination is also interesting for the absence of an extended glycine backbone conformation. For any other amino acid, the succession by proline would have resulted in an extended backbone conformation (*48*), reflected by a large negative $^{13}C^{\alpha}$ secondary shift as seen for the preceding S687-P688 pair. $^{13}C^{\alpha}$ secondary shifts are reported relative to the random coil values of ref *38* but have not been corrected for the approximately +0.5 ppm isotope shift resulting from perdeuteration of the carbon-attached hydrogens. (B) Pico- to nanosecond dynamics, correlative to backbone order (*39*), are compared in the form of heteronuclear {^{1}H}-^{15}N NOE values. Regions that exhibit significant $^{13}C^{\alpha}$ secondary shift differences between bicelle- and micelle-embedded β3 are boxed by blue rectangles.

The close equivalence of the bicelle- and micelle-embedded β3 structure for I693-K716, as well as their divergence for L717-H722, is further illustrated by a comparison of their $^{13}C^{\alpha}$ secondary shifts (Figure 2A). Defined as difference between the observed and tabulated random-coil $^{13}C^{\alpha}$ shift of a residue, secondary $^{13}C^{\alpha}$ chemical shifts correlate well with the underlying backbone conformation (*38*), as evidenced here. The high congruence of the $^{13}C^{\alpha}$ secondary shifts for I693-K716 also indicates that their backbone rmsd of 0.33 Å between bicelle- and micelle-embedded β3 is representative of the accuracy of the obtained structures.

To determine whether the β3 structural differences in the two model membrane systems were related to differences in backbone dynamics, {^{1}H}-^{15}N NOE values were compared. This parameter is sensitive to fluctuations of a residue's backbone H-N bond vector on the pico- to nanosecond time scale, which correlates with backbone order (*39*). Except for a slight variation for S699−V700, this parameter is in close agreement between bicelle- and micelle-

embedded β3 (Figure 2B). Thus, although the α-helical conformation observed for L717-I721 of micelle-embedded β3 is less linear than that found in the bicelle, it is not less ordered. C-terminal to H722, backbone order decreases faster in the micelle than in the bicelle environment. Since the last helix turns of micelle-embedded β3 are distorted, albeit not disordered, helix fraying is probably faster in the micelle compared to the bicelle environment, leading to the faster observed decrease in backbone order. Moreover, for micelle-embedded β3, a kink at D723 was reported (*11, 40*), which would be compatible with the present data. This kink must be a consequence of the micelle environment because H722-D723 are in α-helical conformation in the bicelle environment (Figure 1C and D). On the level of primary structure, the β3 TM domain is also similar to the integrin β2, β5, and β6 subunits (Supporting Information, Figure 3). The described β3 structure can, therefore, serve as a structural template for these integrin subunits.

Assessment of β3 Bicelle/Micelle Embedding. The protection of individual β3 residues from a paramagnetic relaxation agent and solvent–water, respectively, was assessed to examine the embedding of β3 in the bicelle and micelle, respectively. Specifically, backbone H^N resonance-broadening arising from the presence of the relaxation enhancer in the aqueous phase was measured, and the exchange of the backbone H^N nucleus with water was quantified. Water forms a concentration gradient throughout the lipid headgroup region that reaches up to the glycerol backbone of lipids (*41*). A concentration gradient is also present for the employed $Mn^{2+}EDDA^{2-}$ relaxation agent (*42*), but, whereas H^N exchange can be inhibited by intrahelical hydrogen bonding, no such bias exists for the paramagnetic agent. However, the proximity of $Mn^{2+}EDDA^{2-}$ to the backbone H^N nuclei may be somewhat modulated by the surrounding side chains, making the comparison of β3 protection between different hydrophobic environments most useful.

H^N protection from $Mn^{2+}EDDA^{2-}$ is expressed quantitatively as normalized ratio of H-N signal intensities in the presence and absence of the paramagnetic agent, I/I_0. The broadening patterns obtained for bicelle- and micelle-embedded β3 are analogous (Figure 3A), which means that the same residues are embedded in the hydrophobic bicelle/micelle core. The steepest rise in I/I_0 values is obtained between V695 and V696 on the extracellular side and between L718 and I719 on the intracellular side. The central position between these bounds is I707. This residue coincides with the center of the micelle-embedded β3 helix (I693-I721). For the slightly longer helix in the bicelle environment (I693-H722), this indicates that the helix extends farther by one residue on the intra compared to extracellular side. It is also noted that, for both bicelle- and micelle-embedded β3, the rise in I/I_0 values on the extracellular side is steeper than that on the intracellular side, where more residues with intermediate I/I_0 values are present. This may indicate some degree of heterogeneity in the tail-to-headgroup transition of the β3 TM helix or $Mn^{2+}EDDA^{2-}$ concentration gradient on the intracellular side.

The amount of H^N−water exchange taking place during a defined time period is quantified as the ratio of H-N signal intensities obtained with and without the selective inversion of solvent magnetization, I/I_0. On the intracellular side, the different structures of bicelle- and micelle-embedded β3 give

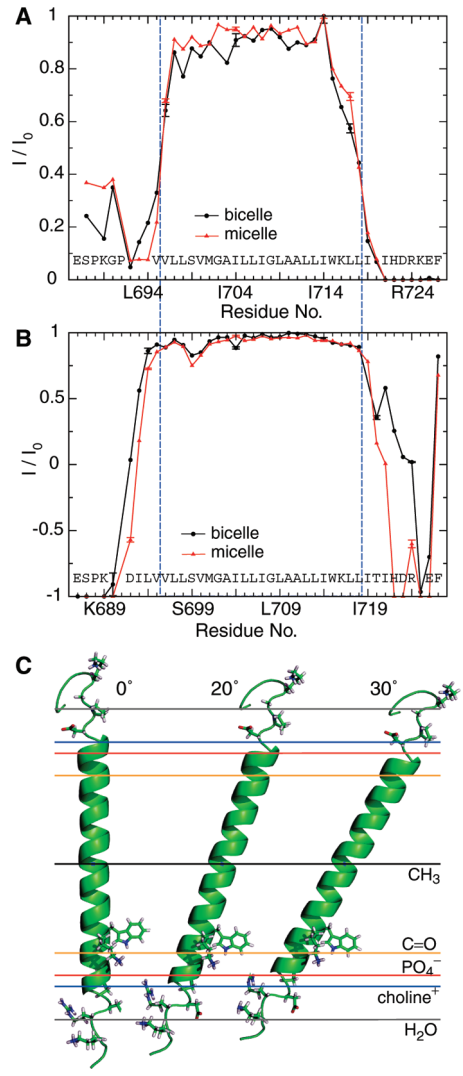

FIGURE 3: Bicelle and micelle embedding of β3. (A) Signal broadening due to paramagnetic relaxation enhancement arising from the presence of $Mn^{2+}EDDA^{2-}$. The normalized ratio of H-N TROSY signal intensities in the presence and absence of 1 mM $Mn^{2+}EDDA^{2-}$, I/I_0, is used to quantify signal broadening for each residue. (B) Exchange of the backbone amide protons (H^N) with water; depicted as the ratio of H-N TROSY signal intensities obtained with and without selective solvent inversion, I/I_0, at pH 8.4 and 25 °C. The solvent was inverted 100 ms prior to the start of the pulse sequence, and radiation damping was suppressed by the application of a weak gradient pulse during this period. An I/I_0 value of −1 corresponds to the exchange of a residue's H^N nucleus with water in all β3 molecules present, whereas a value of +1 denotes the absence of any exchange. Resonances that were absent at pH 8.4, compared to pH 6.5, were assigned I/I_0 values of −1. The water selective pulse (8 ms RE-BURP) is slightly touching the hydroxyl nucleus of S699, which resonates at 4.12 ppm, and an I/I_0 dip ensues in the absence of actual exchange. The same applies to T720, but its hydroxyl nucleus is unobservable and therefore must be in direct, fast exchange with water molecules that reach up to the glycerol lipid backbone (*41*). (C) Structure of the β3 transmembrane helix centered on I707 as a function of the membrane-crossing angle. The experimentally determined average positions of the lipid carbonyl, phosphate, and choline groups (16, 20, and 22 Å from the center of the membrane) are depicted for 1,2-dioleoyl-*sn*-glycero-3-phosphocholine (*41*), which is closely related to the herein employed 1-oleoyl-2-palmitoyl-*sn*-glycero-3-phosphocholine. The bulk water phase is assumed to be fully established at 28 Å (*46*). N-terminal to D692 and C-terminal to D723, the β3 peptide becomes dynamically unstructured, and the depicted conformation for these residues is random.

rise to quite different exchange behaviors (Figure 3B). Much better shielding is observed in the bicelle in agreement with more ideal hydrogen bond geometries (Figure 1C−E) and slower helix fraying (Figure 2B). In the bicelle, complete exchange is observed starting from K725, whereas in the micelle, complete exchange commences at H722. Interestingly, the I/I_0 patterns also differ on the extracellular side where structural differences between bicelle- and micelle-embedded β3 are negligible. In the micelle system, D692 shows almost complete exchange, whereas for the bicelle, this would be expected for P691 (which does not possess an amide proton). This shift in protection by one residue indicates that water can approach the hydrophobic micelle core more closely than the bicelle interior.

Which residues are bordering the micelle and bicelle? On the extracellular side, D692 is the clear candidate. It is the last charged residue before the stretch of (proline-free) hydrophobic residues begins and the first residue to experience rapid H^N−water exchange in the micelle environment. The first charged residue on the intracellular side, K716, clearly is still embedded as shown by its significant protection from $Mn^{2+}EDDA^{2-}$ (Figure 3A). Glycosylation mapping studies of the similar integrin β1 subunit in microsomal membranes have suggested the five residues following β1(K752), L-L-M-I-I, to be membrane embedded (*10*), placing H722 of β3 at the intracellular membrane border. H722 is also the first residue to experience rapid H^N−water exchange in the micelle environment, where it is present in nonhelical conformation. In conclusion, the bicelle and micelle embed the same β3 residues. Solvent exchange, glycosylation mapping studies, and a helix center at residue I707 agree in predicting that residues D692 and H722 border the TM helix on the extra and intracellular side, respectively.

β3 Helix Tilt. While it is not possible to accurately define the β3 membrane-crossing angle with the data at hand, they nevertheless serve to indicate that the β3 transmembrane domain helix will possess a pronounced tilt within a typical lipid bilayer. Figure 3C depicts the orientation of the β3 TM helix centered on I707 relative to the functional groups of a bilayer composed of lipids with 18/18 carbon atom tails (*41*) at three tilt angles. It is evident that a pronounced helix tilt relative to the membrane is required to accommodate the mostly hydrophobic 29-residue TM helix (I693-I721) of approximately 43.5 Å length beyond the charged groups of the lipid molecules. A tilt angle in the range of 20–30° appears likely. A pronounced helix tilt facilitates the snorkeling of K716 by bringing its side chain closer to the headgroup region (Figure 3C) where it can engage a counterion such as a lipid's phosphate group. Similarly, W715's side chain is expected close to the lipids' -CO-O-CHR_2-CH_2- spacer between the headgroup and hydrocarbon tails. Besides tryptophan's general preference for this localization (*43*), the latter statement is supported by its well-defined χ_1 rotamer in the bicelle but not micelle, whose constituent DPC molecules lack the -CO-O-CHR_2-CH_2- spacer. A pronounced helix tilt, therefore, will aid in balancing the opposing immersion tendencies of W715-K716 and L717-I721.

While the same residues are embedded in the micelle than in the bicelle (Figure 3A), the divergence in structures following K716 indicates that a limited plasticity of the micelle constrains the structure of the β3 TM segment on the intracellular side. Specifically, the change in micelle curvature and symmetry imposed by a fully linear α-helical β3 TM structure is apparently not sustainable, leading to L717-I721 deformations (Figure 1C and E). Within the bicelle, the helix tilt places linear α-helical structure for W715-H722 in a nonsymmetrical environment, that is, W715, K716, and I719 are closer to the lipid headgroups, and L717, L718, and I721 are closer to the hydrocarbon tails than they would be at a zero tilt angle (Figures 3C and 1D). This allows K716 to be separated from the membrane border by five residues (L717-I721). When transferring this topography to the micelle environment, a nonzero tilt angle is equivalent to an asymmetric distribution of detergent molecules around the β3 TM helix. The reduction of the overall TM helix length and bending of L717-I721 away from the helix axis toward K716's side chain (Figure 1C and E) may, therefore, have contributions from the lack of a sufficiently asymmetric detergent distribution in addition to curvature strain. It is also interesting to note that micelle curvature and symmetry strains as well as β3 TM helix deformations are not reduced by simply partitioning L717-I721 into the aqueous phase. Apparently, this option is energetically least desirable.

Influence of Lipid Headgroup on β3 Structure. Bicelles possess a symmetrical lipid distribution, which is in contrast to the asymmetric nature of biological membranes. To evaluate the impact of this simplification and to examine the influence of the lipid headgroup type on the β3 TM structure, backbone chemical shifts between different bicelle lipid configurations were compared. In this respect, the backbone ^{15}N chemical shift of a residue is useful since it depends on the underlying backbone and side chain conformations as well as the chemical environment of the amino acid and its surroundings (*44*). To better judge the magnitude of the obtained ^{15}N shift changes upon varying the bicelle lipid headgroup, we first compared the ^{15}N shift differences detected between the bicelle and micelle environment. Large shift changes of up to 2.08 ppm were observed at both helix termini (Figure 4A). On the extracellular side, where β3 structural differences are minimal (Figure 1C), the shift changes reflect changes in the underlying chemical environment. The intracellular side, where β3 structural changes are also significant (Figure 1C), accordingly experiences more widespread ^{15}N shift changes.

Much smaller ^{15}N shift changes were observed between bicelles of different lipid compositions (Figure 4B and C). The introduction of the negatively charged POPG lipid (1-palmitoyl-2-oleoyl-*sn*-glycero-3-[phospho-*rac*-(1-glycerol)]), which is common to plant and prokaryotic cell membranes, was tested in addition to POPS (1-palmitoyl-2-oleoyl-*sn*-glycero-3-[phospho-L-serine]), representing the dominant negatively charged lipid in platelets (*45*). The substitution of one-third of bicellar POPC lipids with POPG lead to significant ^{15}N shift changes only at the C-terminal end of the β3 TM helix (Figure 4B). But even there, the magnitude of the observed shift differences of up to 0.39 ppm is relatively small. The β3 backbone structures in the two bicelle configurations are indistinguishable, as evidenced by the congruence of their $^{13}C^{\alpha}$ secondary shifts (Supporting Information, Figure 4F). Differences in chemical environments, most notably the negative charge of the POPG headgroup and ensuing presence of an external counterion for PO_4^- (*46*), are therefore expected to make the largest

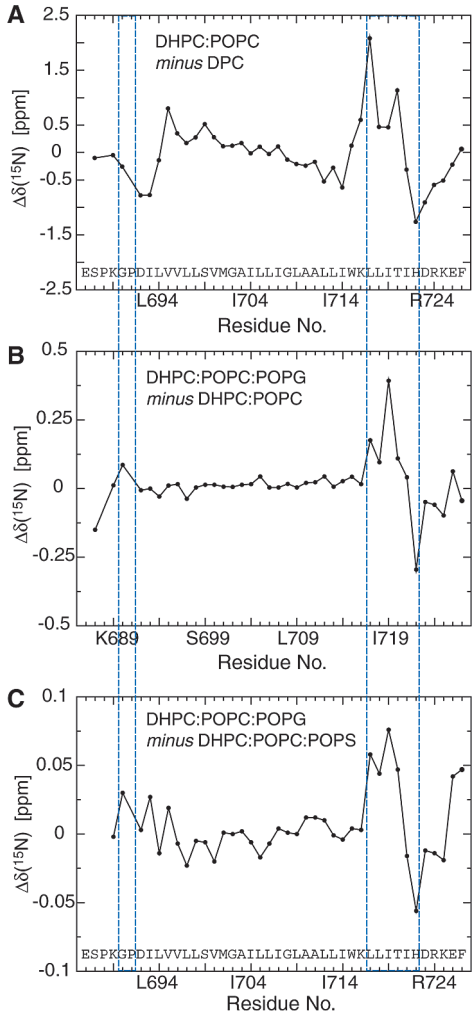

FIGURE 4: Effect of lipid/detergent environment on the β3 backbone ^{15}N chemical shifts. Shift differences are depicted between (A) DHPC:POPC:POPG (350:70:35 mM) and DPC (450 mM); (B) DHPC:POPC:POPG (350:70:35 mM) and DHPC:POPC (350:105 mM); and (C) DHPC:POPC:POPG (350:70:35 mM) and DHPC:POPC:POPS (350:70:35 mM). Note the large differences in *y*-axis scaling. Regions that exhibit significant $^{13}C^{\alpha}$ secondary shift differences between bicelle- and micelle-embedded β3 (Figure 2A) are boxed by blue rectangles.

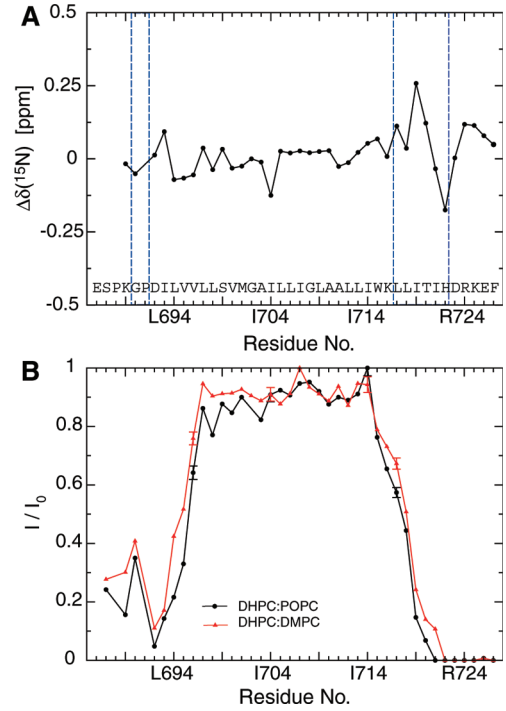

FIGURE 5: Effect of shortening the lipid hydrocarbon tails upon integrin β3 embedding. (A) β3 ^{15}N chemical shift differences between bicelles utilizing lipids with 16/18 carbon atom tails, DHPC:POPC (350:105 mM), and 14/14 atoms tails, DHPC:DMPC (1,2-dimyristoyl-*sn*-glycero-3-phosphocholine; 350:105 mM) are depicted. Regions that exhibit significant $^{13}C^{\alpha}$ secondary shift differences between bicelle- and micelle-embedded β3 (Figure 2A) are boxed by blue rectangles. (B) Comparison of normalized ratio of H-N TROSY signal intensities in the presence and absence of 1 mM $Mn^{2+}EDDA^{2-}$, I/I_0, between β3 embedded in DHPC:POPC and DHPC:DMPC bicelles (each 350:105 mM).

contribution to the ^{15}N shift differences. When substituting POPG for POPS, almost no shift differences were observed (Figure 4C); the maximum deviation of 0.08 ppm is close to the noise. The two bicelle configurations both lead to equivalent β3 structures and provide a highly similar chemical environment for β3. For the sake of completeness, it is noted that backbone $^{1}H^{N}$ shift changes closely follow the detected ^{15}N shift changes (Supporting Information, Figure 4). In sum, the type of headgroup of the glycerophospholipids had a slight impact on the structure of β3 on the intracellular side, but essentially none on the extracellular face. The headgroups can, therefore, be chosen to suit the intracellular β3 side, suggesting that an asymmetric lipid distribution is not required for studying the β3 TM segment.

Implications for Integrin Activation. Separation of integrin α-β subunit TM helices has been proposed as a mechanism for transmitting signals across the bilayer (*2, 4–7*). On the basis of this idea, it would follow that the structure and topology of the monomeric β3 TM helix reported here represent an activated form. In addition, changes in TM helix topology have also been proposed to accompany integrin activation (*9*). TM helix repartitioning is conceivable for the α and/or β subunit. For integrin β3, this would mean transferring L717-I721 out of the hydrophobic bilayer core into the aqueous phase. To investigate the propensity of β3(K716-I721) to partition into the aqueous phase, the tails of the bicelle lipids were shortened from 16/18 to 14/14 carbon atoms. This led to even smaller ^{15}N chemical shift changes than obtained when altering the lipid headgroups (Figure 5A vs Figure 4B). Consistent with these small shift changes, protection from the paramagnetic relaxation agent $Mn^{2+}EDDA^{2-}$ was similar between the bicelles of different lipid tail length (Figure 5B), clearly demonstrating the absence of β3 repartitioning. Thus, monomeric β3 prefers to immerse residues I693-I721 into the hydrophobic cores of all model membrane systems studied here.

The transfer of K716's charged side chain out of the hydrophobic membrane core and the simultaneous immersion of L717-I721 are accomplished by adopting a substantial β3 TM helix tilt relative to the membrane (Figure 3C). The role of the L717-I721 hydrophobic stretch following K716 may, therefore, be to ensure a high propensity for a pronounced β3 TM helix tilt relative to a typical membrane bilayer. The helix tilt angle can specify α-β TM helix packing and thereby control the extent of bidirectional transmembrane signaling. Changes in membrane thickness could also affect integrin signaling by modulating TM helix tilt angles. A substantial increase in lipid tail length could also decrease the tilt angle to a point where K716 snorkeling is not sustainable and,

hence, force L717-I721 repartitioning. On the intracellular side, the β3 TM helix continues into the headgroup region in α-helical conformation before fraying. In the presence of the full-length β3 cytosolic tail, helix propensity continues well into the cytosol (*11, 40, 47*) and the activating talin F3 domain stabilizes helical structure in this membrane-proximal region (*17*). In contrast to the intracellular side, the transition between the β3 TM and extracellular domain is rather abrupt. Preceding D692, the first residue in nonhelical conformation, residues P688-K689-G690-P691 do not show defined structural propensities (Figure 2). While the presence of the β3 extracellular domain may stabilize a particular conformation for P688-P691, the conspicuous abundance of proline and glycine residues is expected to impede the formation of well-defined secondary structure. Thus, the connection between the β3 TM helix and the extracellular domain appears quite different from its connection to the cytoplasmic domain.

SUPPORTING INFORMATION AVAILABLE

A table reporting the β3 structural statistics and a table reporting the χ_1 torsion angle distributions. A figure depicting the H-N correlation spectra of bicelle- and micelle-embedded β3, a figure comparing the H-N chemical shifts of bicelle-embedded β3(P685-F727) and β3(P685-T762), a figure showing the sequence alignment of human integrin β1, β2, β3, β5, and β6 transmembrane segments, and a figure displaying additional β3 chemical shift differences between the different lipid/detergent environments studied. This material is available free of charge via the Internet at http://pubs.acs.org.

REFERENCES

1. Hynes, R. O. (2002) Integrins: Bidirectional, allosteric signaling machines. *Cell 110*, 673–687.
2. Luo, B. H., Springer, T. A., and Takagi, J. (2004) A specific interface between integrin transmembrane helices and affinity for ligand. *PLoS Biol. 2*, 776–786.
3. Hughes, P. E., DiazGonzalez, F., Leong, L., Wu, C. Y., McDonald, J. A., Shattil, S. J., and Ginsberg, M. H. (1996) Breaking the integrin hinge - A defined structural constraint regulates integrin signaling. *J. Biol. Chem. 271*, 6571–6574.
4. Partridge, A. W., Liu, S. C., Kim, S., Bowie, J. U., and Ginsberg, M. H. (2005) Transmembrane domain helix packing stabilizes integrin aIIb beta 3 in the low affinity state. *J. Biol. Chem. 280*, 7294–7300.
5. Li, W., Metcalf, D. G., Gorelik, R., Li, R. H., Mitra, N., Nanda, V., Law, P. B., Lear, J. D., DeGrado, W. F., and Bennett, J. S. (2005) A push-pull mechanism for regulating integrin function. *Proc. Natl. Acad. Sci. U.S.A. 102*, 1424–1429.
6. Vinogradova, O., Velyvis, A., Velyviene, A., Hu, B., Haas, T. A., Plow, E. F., and Qin, J. (2002) A structural mechanism of integrin alpha(IIb)beta(3) "inside-out" activation as regulated by its cytoplasmic face. *Cell 110*, 587–597.
7. Zhu, J. Q., Carman, C. V., Kim, M., Shimaoka, M., Springer, T. A., and Luo, B. H. (2007) Requirement of alpha and beta subunit transmembrane helix separation for integrin outside-in signaling. *Blood 110*, 2475–2483.
8. DiazGonzalez, F., Forsyth, J., Steiner, B., and Ginsberg, M. H. (1996) Trans-dominant inhibition of integrin function. *Mol. Biol. Cell 7*, 1939–1951.
9. Ginsberg, M. H., Partridge, A., and Shattil, S. J. (2005) Integrin regulation. *Curr. Opin. Cell Biol. 17*, 509–516.
10. Armulik, A., Nilsson, I., von Heijne, G., and Johansson, S. (1999) Determination of the border between the transmembrane and cytoplasmic domains of human integrin subunits. *J. Biol. Chem. 274*, 37030–37034.
11. Li, R. H., Babu, C. R., Valentine, K., Lear, J. D., Wand, A. J., Bennett, J. S., and DeGrado, W. F. (2002) Characterization of the monomeric form of the transmembrane and cytoplasmic domains of the integrin beta 3 subunit by NMR spectroscopy. *Biochemistry 41*, 15618–15624.
12. Sanders, C. R., II, and Landis, G. C. (1995) Reconstitution of membrane proteins into lipid-rich bilayered mixed micelles for NMR studies. *Biochemistry 34*, 4030–4040.
13. Vold, R. R., Prosser, R. S., and Deese, A. J. (1997) Isotropic solutions of phospholipid bicelles: a new membrane mimetic for high-resolution NMR studies of polypeptides. *J. Biomol. NMR. 9*, 329–335.
14. Chou, J. J., Kaufman, J. D., Stahl, S. J., Wingfield, P. T., and Bax, A. (2002) Micelle-induced curvature in a water-insoluble HIV-1 Env peptide revealed by NMR dipolar coupling measurement in stretched polyacrylamide gel. *J. Am. Chem. Soc. 124*, 2450–2451.
15. Prosser, R. S., Evanics, F., Kitevski, J. L., and Al-Abdul-Wahid, M. S. (2006) Current applications of bicelles in NMR studies of membrane-associated amphiphiles and proteins. *Biochemistry 45*, 8453–8465.
16. Calderwood, D. A., Yan, B., de Pereda, J. M., Alvarez, B. G. Y., F., Liddington, R. C., and Ginsberg, M. H. (2002) The Phosphotyrosine Binding-like Domain of Talin Activates Integrins. *J. Biol. Chem. 277*, 21749.
17. Wegener, K. L., Partridge, A. W., Han, J., Pickford, A. R., Liddington, R. C., Ginsberg, M. H., and Campbell, I. D. (2007) Structural basis of integrin activation by talin. *Cell 128*, 171–182.
18. Jaroniec, C. P., Kaufman, J. D., Stahl, S. J., Viard, M., Blumenthal, R., Wingfield, P. T., and Bax, A. (2005) Structure and dynamics of micelle-associated human immunodeficiency virus gp41 fusion domain. *Biochemistry 44*, 16167–16180.
19. Tycko, R., Blanco, F. J., and Ishii, Y. (2000) Alignment of biopolymers in strained gels: A new way to create detectable dipole-dipole couplings in high-resolution biomolecular NMR. *J. Am. Chem. Soc. 122*, 9340–9341.
20. Ulmer, T. S., Ramirez, B. E., Delaglio, F., and Bax, A. (2003) Evaluation of backbone proton positions and dynamics in a small protein by liquid crystal NMR spectroscopy. *J. Am. Chem. Soc. 125*, 9179–9191.
21. Ulmer, T. S., Bax, A., Cole, N. B., and Nussbaum, R. L. (2005) Structure and dynamics of micelle-bound human alpha-synuclein. *J. Biol. Chem. 280*, 9595–9603.
22. Chou, J. J., Gaemers, S., Howder, B., Louis, J. M., and Bax, A. (2001) A simple apparatus for generating stretched polyacrylamide gels, yielding uniform alignment of proteins and detergent micelles. *J. Biomol. NMR 21*, 377–382.
23. Delaglio, F., Grzesiek, S., Vuister, G. W., Zhu, G., Pfeifer, J., and Bax, A. (1995) Nmrpipe - a multidimensional spectral processing system based on Unix Pipes. *J. Biomol. NMR 6*, 277–293.
24. Pervushin, K., Riek, R., Wider, G., and Wuthrich, K. (1997) Attenuated T-2 relaxation by mutual cancellation of dipole- dipole coupling and chemical shift anisotropy indicates an avenue to NMR structures of very large biological macromolecules in solution. *Proc. Natl. Acad. Sci. U.S.A. 94*, 12366–12371.
25. Hu, J. S., and Bax, A. (1997) chi(1) angle information from a simple two-dimensional NMR experiment that identifies trans (3)J(NC) gamma couplings in isotopically enriched proteins. *J. Biomol. NMR 9*, 323–328.
26. Kontaxis, G., Clore, G. M., and Bax, A. (2000) Evaluation of cross-correlation effects and measurement of one-bond couplings in proteins with short transverse relaxation times. *J. Magn. Reson. 143*, 184–196.
27. Jaroniec, C. P., Ulmer, T. S., and Bax, A. (2004) Quantitative J correlation methods for the accurate measurement of 13C[prime]-13C[agr] dipolar couplings in proteins. *J. Biomol. NMR 30*, 181–194.
28. Chou, J. J., Delaglio, F., and Bax, A. (2000) Measurement of one-bond N-15-C-13 ′ dipolar couplings in medium sized proteins. *J. Biomol. NMR 18*, 101–105.
29. Schwieters, C. D., Kuszewski, J. J., Tjandra, N., and Clore, G. M. (2003) The Xplor-NIH NMR molecular structure determination package. *J. Magn. Reson. 160*, 65–73.
30. Cornilescu, G., Delaglio, F., and Bax, A. (1999) Protein backbone angle restraints from searching a database for chemical shift and sequence homology. *J. Biomol. NMR 13*, 289–302.
31. Grishaev, A., and Bax, A. (2004) An empirical backbone-backbone hydrogen-bonding potential in proteins and its applications to NMR structure refinement and validation. *J. Am. Chem. Soc. 126*, 7281–7292.

32. Kuszewski, J. J., and Clore, G. M. (2000) Sources of and solutions to problems in the refinement of protein NMR structures against torsion angle potentials of mean force. *J. Magn. Reson. 146*, 249–254.
33. Gray, T. M., and Matthews, B. W. (1984) Intrahelical hydrogen-bonding of serine, threonine and cysteine residues within alpha-helices and its relevance to membrane-bound proteins. *J. Mol. Biol. 175*, 75–81.
34. Chamberlain, A. K., and Bowie, J. U. (2004) Analysis of side-chain rotamers in transmembrane proteins. *Biophys. J. 87*, 3460–3469.
35. Li, R. H., Babu, C. R., Lear, J. D., Wand, A. J., Bennett, J. S., and DeGrado, W. F. (2001) Oligomerization of the integrin alpha llb beta 3: Roles of the transmembrane and cytoplasmic domains. *Proc. Natl. Acad. Sci. U.S.A. 98*, 12462–12467.
36. Schneider, D., and Engelman, D. M. (2004) Involvement of transmembrane domain interactions in signal transduction by alpha/beta integrins. *J. Biol. Chem. 279*, 9840–9846.
37. Tjandra, N., and Bax, A. (1997) Direct measurement of distances and angles in biomolecules by NMR in a dilute liquid crystalline medium. *Science 278*, 1111–1114.
38. Spera, S., and Bax, A. (1991) Empirical correlation between protein backbone conformation and C-alpha and C-beta C-13 nuclear-magnetic-resonance chemical-shifts. *J. Am. Chem. Soc. 113*, 5490–5492.
39. Lipari, G., and Szabo, A. (1982) Model-free approach to the interpretation of nuclear magnetic- resonance relaxation in macromolecules. 1. Theory and range of validity. *J. Am. Chem. Soc. 104*, 4546–4559.
40. Vinogradova, O., Vaynberg, J., Kong, X. M., Haas, T. A., Plow, E. F., and Qin, J. (2004) Membrane-mediated structural transitions at the cytoplasmic face during integrin activation. *Proc. Natl. Acad. Sci. U.S.A. 101*, 4094–4099.
41. Wiener, M. C., and White, S. H. (1992) Structure of a fluid dioleoylphosphatidylcholine bilayer determined by joint refinement of X-ray and neutron-diffraction data. 3. Complete structure. *Biophys. J. 61*, 434–447.
42. Altenbach, C., Greenhalgh, D. A., Khorana, H. G., and Hubbell, W. L. (1994) A collision gradient-method to determine the immersion depth of nitroxides in lipid bilayers - application to spin-labeled mutants of bacteriorhodopsin. *Proc. Natl. Acad. Sci. U.S.A. 91*, 1667–1671.
43. Yau, W. M., Wimley, W. C., Gawrisch, K., and White, S. H. (1998) The preference of tryptophan for membrane interfaces. *Biochemistry 37*, 14713–14718.
44. Wang, Y. J., and Jardetzky, O. (2004) Predicting N-15 chemical shifts in proteins using the preceding residue-specific individual shielding surfaces from phi, psi(i-1), and chi(1) torsion angles. *J. Biomol. NMR 28*, 327–340.
45. GarciaGuerra, R., GarciaDominguez, J. A., and GonzalezRodriguez, J. (1996) A new look at the lipid composition of the plasma membrane of human blood platelets relative to the GPIIb/IIIa (integrin alpha IIb beta 3) content. *Platelets 7*, 195–205.
46. Zhao, W., Rog, T., Gurtovenko, A. A., Vattulainen, I., and Karttunen, M. (2007) Atomic-scale structure and electrostatics of anionic palmitoyloleoylphosphatidylglycerol lipid bilayers with Na+ counterions. *Biophys. J. 92*, 1114–1124.
47. Ulmer, T. S., Yaspan, B., Ginsberg, M. H., and Campbell, I. D. (2001) NMR analysis of structure and dynamics of the cytosolic tails of integrin alpha IIb beta 3 in aqueous solution. *Biochemistry 40*, 7498–7508.
48. Karplus, P. A. (1996) Experimentally observed conformation-dependent geometry and hidden strain in proteins. *Protein Sci. 5*, 1406–1420.

BI800107A